九州大学学術情報リポジトリ
Kyushu University Institutional Repository

Numerical computations of cavity flow problems by a pressure stabilized characteristic-curve finite element scheme

Notsu, Hirofumi
Faculty of Mathematics, Kyushu University

https://hdl.handle.net/2324/12549

出版情報：日本計算工学会論文集. 2008, pp.20080032-, 2008-12-26. Japan Society for Computational Engineering and Science
バージョン：
権利関係：

KYUSHU UNIVERSITY

MI Preprint Series

Kyushu University
The Grobal COE Program
Math-for-Industry Education & Research Hub

Numerical computations of cavity flow problems by a pressure stabilized characteristic-curve finite element scheme

Hirofumi NOTSU

MI 2008-4

(Received October 16, 2008)

Faculty of Mathematics
Kyushu University
Fukuoka, JAPAN

Numerical computations of cavity flow problems by a pressure stabilized characteristic-curve finite element scheme

Hirofumi NOTSU[1]

[1] Faculty of Mathematics, Kyushu University (Hakozaki, Fukuoka 812-8581, Japan)

Abstract We apply a newly developed characteristic-curve finite element scheme to cavity flow problems. The scheme is useful for large scale computation, because P1/P1 element is employed and the matrix of resulting linear system is symmetric. Numerical results of two- and three-dimensional cavity flow problems are presented. Three types of the Dirichlet boundary condition, discontinuous, C^0 and C^1 continuous ones, are treated, and the difference of the solutions is discussed.

Keywords **:** finite element method, characteristic-curve, pressure stabilization, the Navier-Stokes equations, cavity flow problem

1 Introduction

In this paper we present numerical results of cavity flow problems by a newly developed characteristic-curve finite element scheme[17]. The classical cavity flow problem, whose Dirichlet boundary condition is given by a discontinuous function, is well known as a benchmark one for incompressible fluid flows. Many authors solve the problem, such as Cruchaga and Oñate[5], Ghia et al.[8], Kondo et al.[12], Nallasamy and Prasad[15], Tabata and Fujima[23] in 2D, Fujima et al.[7], Iwatsu et al.[10], Jiang et al.[11], Ku et al.[13] in 3D, and so on. We compute the problem in 2D too.

However, we have some doubt on solving the classical cavity flow problem, because the problem has no weak solution. Therefore, we also compute two other cavity flow problems in 2D and 3D, which are regularized by C^0 and C^1 continuous functions to be used for the Dirichlet boundary condition.

The characteristic-curve method is based on an approximation of the material derivative along the trajectory of the fluid particle, and is natural from the physical point of view. The method has an advantage that the matrix for the system of linear equations is symmetric, which leads to symmetric linear solvers.

Several characteristic-curve finite element schemes for the Navier-Stokes equations of first and second order in time have been developed by Boukir et al.[2], the author and Tabata[16], Pironneau[18]·[19] and Süli[21]. These schemes impose the inf-sup condition[4]·[9] for the finite elements to be used, e.g., P2/P1 element, which requires large memory.

Recently a pressure stabilized characteristic-curve finite element scheme for the Navier-Stokes equations has been proposed by the author and Tabata[17]. The scheme employs a cheap element P1/P1, i.e., velocity and pressure are both approximated by the piecewise linear elements in triangles (2D) or tetrahedra (3D). The P1/P1 element is useful especially in three-dimensional computation. Since the P1/P1 element does not satisfy the inf-sup condition, a pressure stabilization method by Brezzi and Douglas Jr.[3] is used. The scheme is an implicit and mixed one. It has been shown that the numerical convergence order to an exact solution is first in both time and space in the paper[17]. The scheme has such advantages that the matrix is symmetric and that it is useful for large scale computation. Considering to find a stationary solution of the nonstationary Navier-Stokes equations, we apply the scheme to cavity flow problems.

For a domain $\Omega \subset \mathbb{R}^d\,(d=2,3)$ we use the Sobolev spaces $L^2(\Omega)$ and $H^1(\Omega)$, and their subspace

$$L_0^2(\Omega) \equiv \left\{ q \in L^2(\Omega);\ \int_\Omega q\,dx = 0 \right\}.$$

We denote by $(\cdot,\cdot)$ the $L^2(\Omega)$-inner products in the scalar-, vector- and matrix-valued function spaces, by $\|\cdot\|_0$ their norms and by $\|\cdot\|_1$ the norm in $H^1(\Omega)^d$. The dual pairing between a space X and the dual space X' is denoted by $\langle\cdot,\cdot\rangle$.

The outline of this paper is as follows. We set cavity flow problems in Section 2. A pressure stabilized characteristic-curve finite element scheme for the Navier-Stokes equations is reviewed in Section 3. In Section 4 we show numerical results of two- and three-dimensional cavity flow problems.

2 Cavity flow problems

Let $\Omega \subset \mathbb{R}^d\,(d=2,3)$ be a bounded domain and $\Gamma \equiv \partial\Omega$ be the boundary of Ω. We consider the stationary Navier-Stokes problem subject to the Dirichlet boundary condition; find $(u,\ p) : \Omega \to \mathbb{R}^d \times \mathbb{R}$ such that

$$\begin{cases} (u\cdot\nabla)u - \dfrac{2}{Re}\nabla D(u) + \nabla p = f & \text{in } \Omega, \\ \nabla\cdot u = 0 & \text{in } \Omega, \\ u = g & \text{on } \Gamma, \end{cases} \tag{1}$$

where u is the velocity, p is the pressure, Re is the Reynolds number, f is an external force, $D(u)$ is the strain-rate tensor defined by

$$D_{ij}(u) \equiv \frac{1}{2}\Big(\frac{\partial u_i}{\partial x_j} + \frac{\partial u_j}{\partial x_i}\Big) \quad (i,j = 1,\cdots,d)$$

and

$$\big[\nabla D(u)\big]_i \equiv \sum_{j=1}^{d} \frac{\partial D_{ij}(u)}{\partial x_j} \quad (i = 1,\cdots,d).$$

2.1 Two- and three-dimensional cavity flow problems

For cavity flow problems the domain $\Omega \equiv (0,\ 1)^d$ is an unit square or cube and $f \equiv 0$. We set two-dimensional cavity flow problems with four Dirichlet boundary conditions.

Problem 1 (2D)**.** *In* (1) *we take* $Re = 100,\ 1{,}000$ *and* $5{,}000$*, and consider four boundary conditions as follows (see Fig. 1).*

$$g_1(x) = \begin{cases} 1 & (x_1 \neq 0,1,\ x_2 = 1) \\ 0 & (otherwise) \end{cases}, \quad g_2 = 0, \qquad \text{(DC0)}$$

$$g_1(x) = \begin{cases} 1 & (x_2 = 1) \\ 0 & (otherwise) \end{cases}, \quad g_2 = 0, \qquad \text{(DC1)}$$

$$g_1(x) = \begin{cases} 4x_1(1-x_1) & (x_2 = 1) \\ 0 & (otherwise) \end{cases}, \quad g_2 = 0, \quad \text{(C0)}$$

$$g_1(x) = \begin{cases} \big\{4x_1(1-x_1)\big\}^2 & (x_2 = 1) \\ 0 & (otherwise) \end{cases}, \quad g_2 = 0. \qquad \text{(C1)}$$

The problem with the boundary condition (DC0) or (DC1) is known as a benchmark one. The difference between the boundary conditions (DC0) and (DC1) is the values of g_1 at only two corners $(x_1,x_2) = (0,1)$ and $(1,1)$. In the cases of the boundary conditions (DC0) and (DC1), there does not exist a weak solution, i.e., $(u,p) \notin H^1(\Omega)^2 \times L^2(\Omega)$. But we set these problems to compare with the preceding results by Ghia et al.[8] and see the the difference of values of g_1 at the two corners. We can regularize these problems by considering the boundary conditions (C0) or (C1).

Below is three-dimensional cavity flow problems with C^0 and C^1 continuous types of the Dirichlet boundary condition.

Problem 2 (3D)**.** *In* (1) *we take* $Re = 100,\ 400$ *and* $1{,}000$*, and consider two boundary conditions as follows (see Fig. 2).*

$$g_1(x) = \begin{cases} 16x_1(1-x_1)x_2(1-x_2) & (x_3 = 1) \\ 0 & (otherwise) \end{cases},$$
$$g_2 = g_3 = 0, \qquad \text{(C0-3D)}$$

$$g_1(x) = \begin{cases} \big\{16x_1(1-x_1)x_2(1-x_2)\big\}^2 & (x_3 = 1) \\ 0 & (otherwise) \end{cases},$$
$$g_2 = g_3 = 0. \qquad \text{(C1-3D)}$$

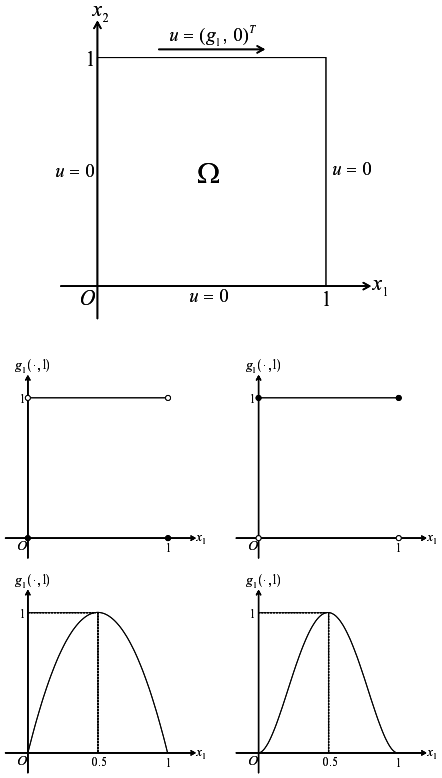

Figure 1: An image of cavity flow problems in 2D (top) and graphs of $g_1(\cdot,1)$ for the boundary conditions (DC0) (middle left), (DC1) (middle right), (C0) (bottom left) and (C1) (bottom right).

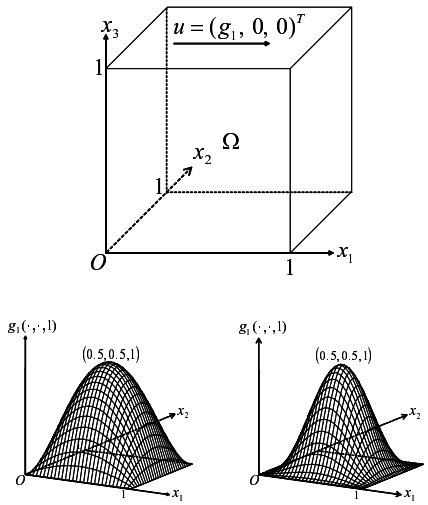

Figure 2: An image of cavity flow problems in 3D (top) and graphs of $g_1(\cdot,\cdot,1)$ for the boundary conditions (C0-3D) (bottom left) and (C1-3D) (bottom right).

3 Review of a pressure stabilized characteristic-curve finite element scheme

In this section we review a pressure stabilized characteristic-curve finite element scheme for the Navier-Stokes equations in the paper[17].

Let T be a positive constant. We consider the non-stationary Navier-Stokes problem subject to the Dirichlet boundary condition; find $(u,\ p) : \Omega \times (0,T) \to \mathbb{R}^d \times \mathbb{R}$ such that

$$\begin{cases} \dfrac{\partial u}{\partial t} + (u\cdot\nabla)u - \dfrac{2}{Re}\nabla D(u) + \nabla p = f & \text{in } \Omega\times(0,T), \\ \nabla\cdot u = 0 & \text{in } \Omega\times(0,T), \\ u = g & \text{on } \Gamma\times(0,T), \\ u = u^0 & \text{in } \Omega, \text{ at } t=0. \end{cases} \tag{2}$$

We assume $f = f(x,t)$ and $g = g(x,t)$ only in this section to review the scheme for such general functions.

3.1 An idea of a characteristic-curve method

We explain an idea of a characteristic-curve method of first order in time simply.

Let Δt be a time increment and $N_T \equiv [T/\Delta t]$ be a total step number. We set $t^n \equiv n\Delta t$ for $n \in \mathbb{N}\cup\{0\}$. For a function ϕ on $\Omega\times(0,T)$ or $\Gamma\times(0,T)$ and an integer n $(0 \le n \le N_T)$, ϕ^n means $\phi^n \equiv \phi(\cdot,t^n)$. For a velocity $w : \Omega \to \mathbb{R}^d$, we define $X_1(w,\Delta t) :\ \Omega \to \mathbb{R}^d$ by

$$X_1(w,\Delta t)(x) \equiv x - w(x)\Delta t.$$

We use the symbol $\circ$ to designate the composition of functions, e.g., for a function ϕ defined in Ω

$$\big(\phi\circ X_1(w,\Delta t)\big)(x) \equiv \phi(X_1(w,\Delta t)(x)).$$

Let $u : \Omega\times(0,T) \to \mathbb{R}^d$ be a smooth function and $X : (0,T) \to \mathbb{R}^d$ be a solution of the ordinary differential equation,

$$\begin{cases} X'(t) = u(X,t) & \text{in } (t^{n-1},t^n), \\ X(t^n) = x, \end{cases} \tag{3}$$

for a point $x \in \Omega$ and an integer n $(1 \le n \le N_T)$. Then, the material derivative of a smooth function $\phi :\ \Omega\times(0,T) \to \mathbb{R}$ at $t = t^n$ is approximated as follows;

$$\begin{aligned} \Big(\frac{\partial}{\partial t} + u\cdot\nabla\Big)\phi(x,t) &= \frac{d}{dt}\phi(X(t),t) \\ &= \frac{\phi^n(X(t^n)) - \phi^{n-1}(X(t^{n-1}))}{\Delta t} + O(\Delta t) \\ &= \frac{\phi^n - \phi^{n-1}\circ X_1(u^{n-1},\Delta t)}{\Delta t}(x) + O(\Delta t), \end{aligned} \tag{4}$$

where we have used the relation,

$$X(t^{n-1}) = X_1(u^{n-1},\Delta t)(x) + O(\Delta t^2).$$

For the Navier-Stokes equations, substituting u_i $(i = 1,\cdots,d)$ into ϕ in (4), we get the approximation of the material derivative of u at $t = t^n$,

$$\Big(\frac{\partial u}{\partial t} + (u\cdot\nabla)u\Big)(x,t) = \frac{u^n - u^{n-1}\circ X_1(u^{n-1},\Delta t)}{\Delta t}(x) + O(\Delta t).$$

3.2 A finite element scheme

Let $\mathscr{T}_h \equiv \{K\}$ be a triangulation of Ω, where subscript h means representative length of the triangulation. We define Ω_h by

$$\Omega_h \equiv \text{int}\bigcup\{K;\ K\in\mathscr{T}_h\}$$

and the boundary $\Gamma_h \equiv \partial\Omega_h$. For a vector valued function g on Γ we set finite element spaces,

$$\begin{aligned} X_h &\equiv \big\{v_h \in C^0(\overline{\Omega}_h)^d;\ v_h|_K \in P_1(K)^d,\ \forall K\in\mathscr{T}_h\big\}, \\ M_h &\equiv \big\{q_h \in C^0(\overline{\Omega}_h);\ q_h|_K \in P_1(K),\ \forall K\in\mathscr{T}_h\big\}, \\ V_h(g) &\equiv \big\{v_h \in X_h;\ v_h(P) = g(P),\ \forall P\in\Gamma_h\big\}, \\ V_h &\equiv V_h(0), \quad Q_h \equiv M_h\cap L^2_0(\Omega_h), \end{aligned} \tag{5}$$

where P is any nodal point on Γ_h. Let Π_h be the interpolation operator from $C^0(\overline{\Omega}_h)^d$ to X_h. For an external force $f \in C^0(\overline{\Omega}\times[0,T])^d$, f_h^n means $\Pi_h f^n$. For $u, w \in H^1(\Omega_h)^d$ we define linear forms $\mathscr{M}_h(u,w,\Delta t)$ and $\mathscr{F}_h^n$ on V_h,

$$\begin{aligned} \langle\mathscr{M}_h(u,w;\Delta t),\ v_h\rangle &\equiv \Big(\frac{u - w\circ X_1(w,\Delta t)}{\Delta t},\ v_h\Big), \\ \langle\mathscr{F}_h^n,\ v_h\rangle &\equiv \big(f_h^n,\ v_h\big), \end{aligned}$$

and bilinear forms a_h, b_h and $\mathscr{C}_h$ on $H^1(\Omega_h)^d \times H^1(\Omega_h)^d$, $H^1(\Omega_h)^d\times L^2(\Omega_h)$ and $H^1(\Omega_h)\times H^1(\Omega_h)$, respectively,

$$\begin{aligned} a_h(u,v) &\equiv \frac{2}{Re}\big(D(u),\ D(v)\big), \\ b_h(v,q) &\equiv -\big(\nabla\cdot v,\ q\big), \\ \mathscr{C}_h(p,q) &\equiv -\delta\sum_{K\in\mathscr{T}_h} h_K^2\big(\nabla p,\ \nabla q\big)_K. \end{aligned}$$

Here δ is a positive constant, h_K is the diameter of element K and $(\cdot,\cdot)_K$ represents the L^2-inner product on element K.

We write the scheme for (2) in the paper[17] again; find $\{(u_h^n,\ p_h^n) \in V_h(g^n)\times Q_h;\ n = 1,\cdots,N_T\}$ such that, for $n = 1,\cdots,N_T$,

$$\begin{aligned} &\langle\mathscr{M}_h(u_h^n,u_h^{n-1};\Delta t),v_h\rangle + a_h(u_h^n,v_h) + b_h(v_h,p_h^n) \\ &\quad + b_h(u_h^n,q_h) + \mathscr{C}_h(p_h^n,q_h) = \langle\mathscr{F}_h^n,\ v_h\rangle, \\ &\quad \forall (v_h,q_h) \in V_h\times Q_h, \end{aligned} \tag{6}$$

where u_h^0 is a function approximating u^0.

Using the same given functions f and g in (1) for (2) and solving the scheme (6), we find a numerical stationary solution of (2) as a solution of (1).

Remark 1. *In cases of solving cavity flow problems, $\Omega = \Omega_h$, $\Gamma = \Gamma_h$, $f = 0$ and $g = g(x)$.*

Remark 2. *For cavity flow problems, we set u^0 as the solution of the stationary Stokes equations with the same boundary condition $u = g$ on Γ. Since u^0 is not given explicitly, we compute the solution $(w_h, r_h) \in V_h(g) \times Q_h$ of the problem;*

$$\tilde{a}_h(w_h, v_h) + b_h(v_h, r_h) + b_h(w_h, q_h) + \mathscr{C}_h(r_h, q_h) = 0, \quad \forall (v_h, q_h) \in V_h \times Q_h, \qquad (7)$$

where $\tilde{a}_h$ is a_h with $Re = 1$, and set $u_h^0 \equiv w_h$.

4 Numerical results

In this section we show two- and three-dimensional numerical results of cavity flow problems by the scheme (6). The scheme has numerical convergence order $O(h + \Delta t)$ to exact solutions, which has been recognized for Examples 1 and 3 in the paper[17]. Therefore, if there exists a (sufficiently smooth) unique solution of (2), we can expect the solution by the scheme to converge to the exact one as h and Δt go to 0.

We use the CR method[14] with the point Jacobi preconditioner[1] for solving the system of linear equations, which works for our symmetric matrix. In the scheme we have to compute a integral,

$$\int_K u_h^{n-1} \circ X_1(u_h^{n-1}, \Delta t) v_h \, dx$$

on triangular elements K. The integrand

$$u_h^{n-1} \circ X_1(u_h^{n-1}, \Delta t) v_h$$

is not smooth on K. It is known that rough numerical integration causes oscillation even in the case that the stability is theoretically proved for a scheme with exact integration, see the papers by Tabata[22] and Tabata and Fujima[24]. The two solutions using numerical integration formula of degree two (2D: three points, 3D: four points) and five (2D: seven points, 3D: fifteen points)[20] are almost same for Examples 1 and 3 in the paper[17]. Therefore, in all the following computations we use the numerical integration formula of degree two.

Let N_Ω be the division number of each side of Ω, (u, p) and (u_h, p_h) be the solutions of the problem (2) and the scheme (6), respectively, and $n_t \equiv [t/\Delta t]$ be the step number for $t \in \mathbb{N}$. Setting a norm

$$\|(v,\, q)\|_{H^1 \times L^2} \equiv \frac{1}{\sqrt{Re}} \|v\|_1 + \|q\|_0$$

in the product space $H^1(\Omega)^d \times L^2(\Omega)$, for $t \in \mathbb{N} \setminus \{1\}$ we define $Diff_t$ by

$$Diff_t \equiv \frac{\|(u_h^{n_t}, p_h^{n_t}) - (u_h^{n_{t-1}}, p_h^{n_{t-1}})\|_{H^1 \times L^2}}{\|(u_h^{n_{t-1}}, p_h^{n_{t-1}})\|_{H^1 \times L^2}},$$

which represents a difference of the solution at times t and $t-1$. We set $\delta = 0.2$ and 0.05 for 2D and 3D problems, respectively. These values are the same as the ones in the paper[17].

4.1 Two-dimensional cavity flow problems, Problem 1

In this subsection we show numerical results for Problem 1.

We used FreeFem++[6] for mesh generation. Considering the boundary layers, we used nonuniform meshes refined near the boundary. Fig. 3 shows the meshes, and we call the meshes Fine and Coarse meshes, respectively. These two meshes are similar around the center of the domain. The discretization parameters for the meshes are shown in Table 1, where $h_{\min}$ is a minimum element size. Table 2 shows values of Δt used for Problem 1. For high Reynolds number problems an approximation of the nonlinear convection term is important. In the scheme, the approximation depends on not only h but also Δt. This is the reason why we change the values of Δt according to the Reynolds numbers.

Table 1: Discretization parameters for meshes in Fig 3.

Mesh	♯ of nodes	♯ of elements	$h_{\min}$
Fine	11,470	21,914	2.76×10^{-3}
Coarse	5,403	10,282	5.52×10^{-3}

Table 2: Values of Δt used for Problem 1.

	Δt	
Re	Fine mesh	Coarse mesh
100	1/100	1/50
1,000	1/200	1/100
5,000	1/800	1/400

The numerical solutions converged to stationary solutions in the sense of satisfying the inequality

$$Diff_t < 10^{-5}. \qquad (8)$$

The times of convergence are listed in Table 3. Since we have defined $Diff_t$ for only $t \in \mathbb{N} \setminus \{1\}$, the times in the table are integers. For each Re, Figs. 4, 6 and 8 and Figs. 5, 7 and 9 show the graphs of $u_{h1}(0.5, \cdot)$ and $u_{h2}(\cdot, 0.5)$ of the two stationary solutions on Fine and Coarse meshes and the streamlines of stationary solutions on Fine mesh, respectively. For the boundary conditions (DC0) and (DC1), we plot the results by Ghia et al.[8] in the graphs. In the cases of the boundary conditions (C0) and (C1), the graphs by the two stationary solutions are almost same, and the streamlines exhibit the flow patterns well.

In the cases of the boundary conditions (DC0) and (DC1), although there does not exist a weak solution, the numerical solution exists. For $Re = 100$ and $1,000$ of (DC0) and $Re = 100$ of (DC1), the graphs by the two stationary solutions are almost same and are similar to the results by Ghia et al. For $Re = 5,000$ of (DC0) and $Re = 1,000$ and $5,000$ of (DC1), there are differences in the graphs by the two stationary solutions, and the solutions on Fine mesh are more close to the results by Ghia

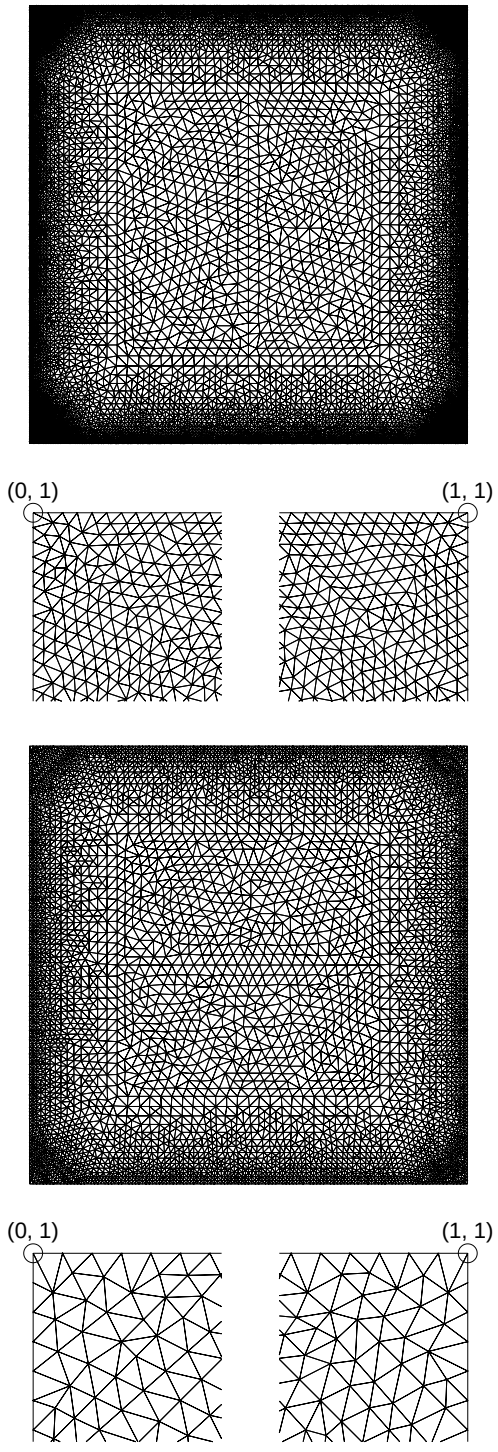

Figure 3: Meshes used for Problem 1, Fine mesh ($N_\Omega = 256$), the mesh magnified around the corners $(x_1, x_2) = (0,1)$ and $(1,1)$, Coarse mesh ($N_\Omega = 128$) and the mesh magnified around the corners (top to bottom).

et al. than ones on Coarse mesh. The difference between the boundary conditions is the values of g_1 at only two corners $(x_1, x_2) = (0,1)$ and $(1,1)$. However, there are evident differences of the streamlines by the two boundary conditions in the three Figs. 5, 7 and 9. The similar results have been reported by Cruchaga and Oñate[5]. They have shown the comparison of graphs of $u_{h1}(0.5,\cdot)$ and $u_{h2}(\cdot, 0.5)$ for (DC0) and (DC1) with $Re = 1,000,\ 5,000$ and $10,000$.

Table 3: Convergence times.

		$t\ (\in \mathbb{N})$	
	Re	Fine mesh	Coarse mesh
(DC0):	100	15	15
	1,000	85	92
	5,000	370	358
(DC1):	100	15	15
	1,000	87	87
	5,000	352	399
(C0):	100	16	16
	1,000	92	91
	5,000	372	373
(C1):	100	17	17
	1,000	91	90
	5,000	356	360

4.2 Three-dimensional cavity flow problems, Problem 2

In this subsection we show numerical results for Problem 2. The finite element subdivision of the domain is constructed by dividing the domain into a union of triangular prisms and further subdividing each triangular prism into three tedrahedra. In this process, a triangular mesh of the two-dimensional domain $\omega \equiv (0,1)^2$ by FreeFem++ is used.

Considering the boundary layers, we used nonuniform two meshes in Fig. 10. We call the meshes Fine and Coarse meshes, respectively, whose discretization parameters are shown in Table 4. In three-dimensional case, for all the Reynolds numbers we set $\Delta t = 1/32$ for Fine mesh and $\Delta t = 1/24$ for Coarse mesh.

The numerical solutions converged to stationary solutions in the sense of satisfying the inequality (8). The times of convergence are listed in Table 5. Figs. 11, 15 and 19 show the graphs of $u_{h1}(0.5, 0.5, \cdot)$ and $u_{h3}(\cdot, 0.5, 0.5)$ of the two stationary solutions on Fine and Coarse meshes for the two boundary conditions (C0-3D) and (C1-3D) for each *Re*. The graphs of the two stationary solutions are almost same. Figs. 12–14, 16–18 and 20–22 are projections of velocity vectors on each plane for each *Re*, which exhibit the flow patterns well of these problems.

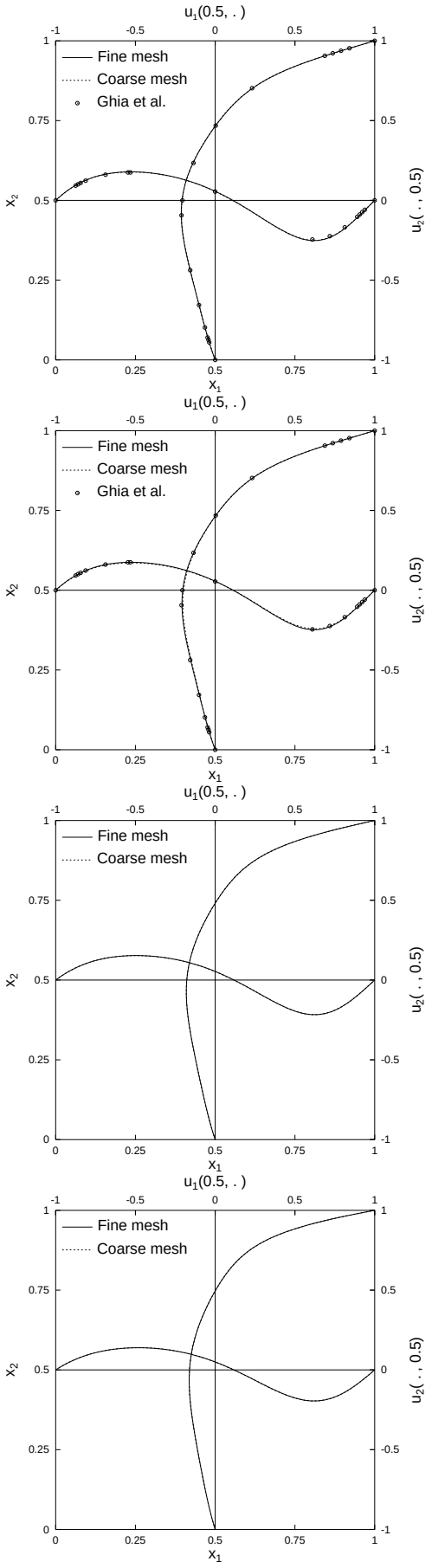

Figure 4: Graphs of $u_{h1}(0.5,\cdot)$ and $u_{h2}(\cdot,0.5)$, $Re = 100$, (DC0), (DC1), (C0) and (C1) (top to bottom).

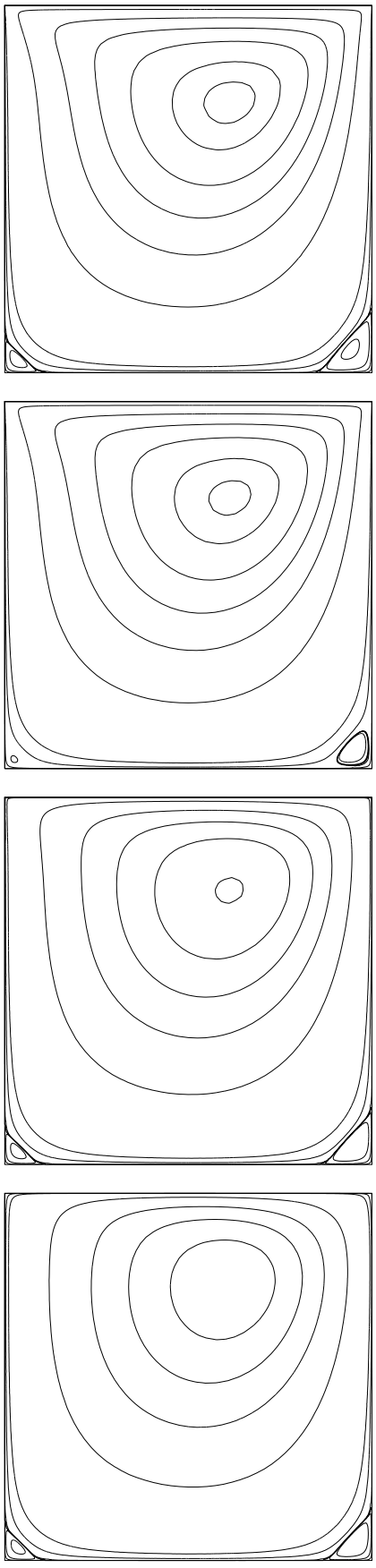

Figure 5: Streamlines, $Re = 100$, (DC0), (DC1), (C0) and (C1) (top to bottom).

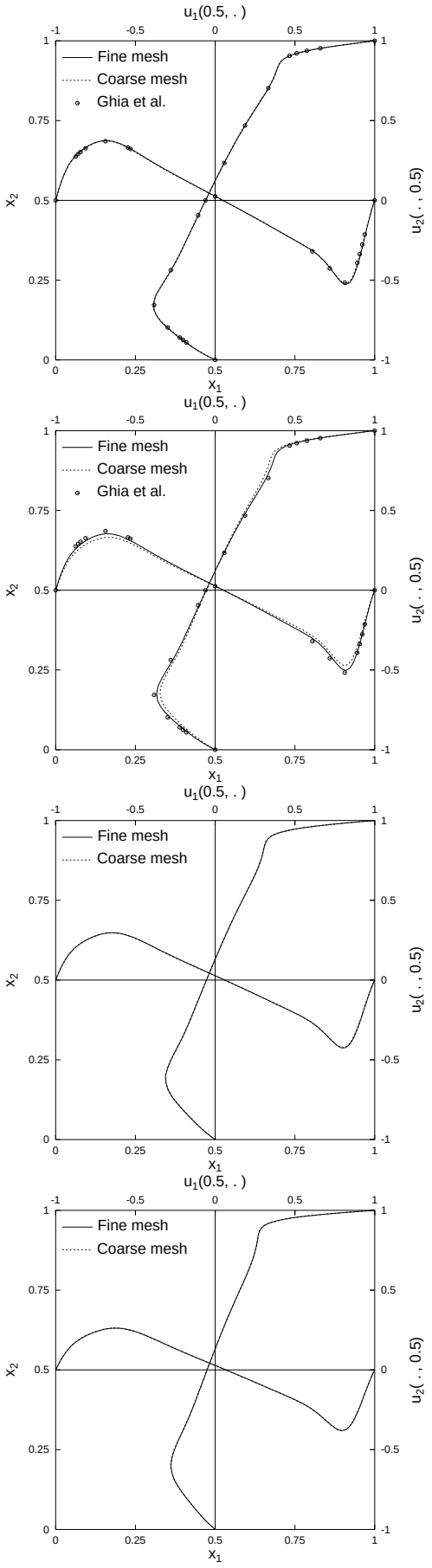

Figure 6: Graphs of $u_{h1}(0.5,\cdot)$ and $u_{h2}(\cdot,0.5)$, $Re = 1,000$, (DC0), (DC1), (C0) and (C1) (top to bottom).

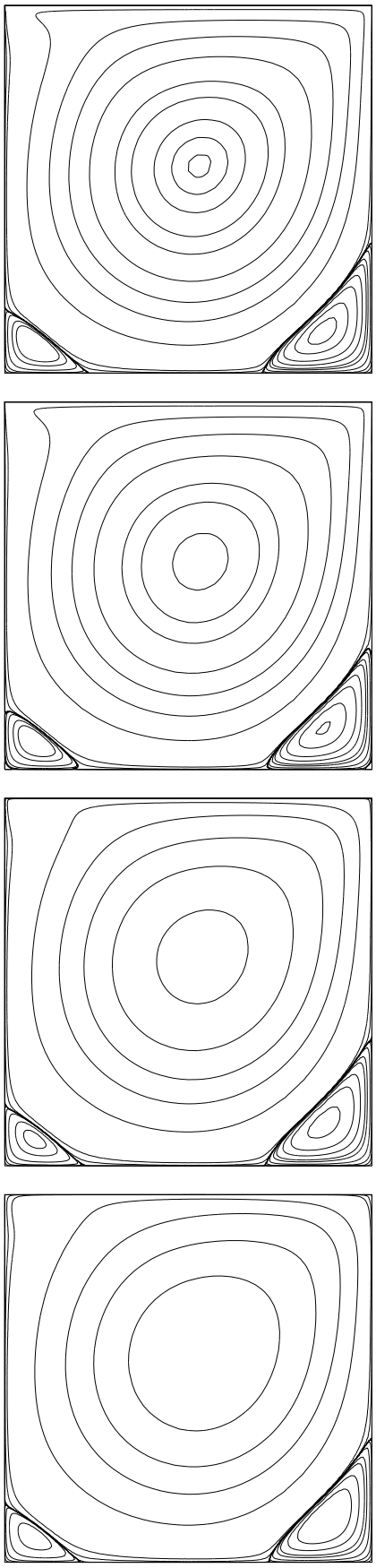

Figure 7: Streamlines, $Re = 1,000$, (DC0), (DC1), (C0) and (C1) (top to bottom).

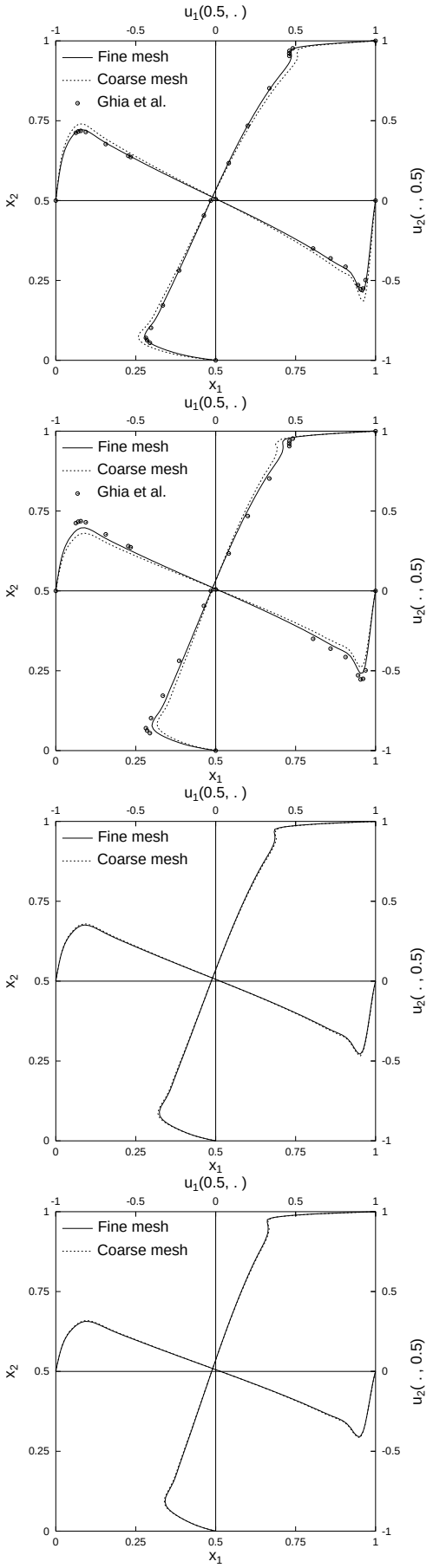

Figure 8: Graphs of $u_{h1}(0.5,\cdot)$ and $u_{h2}(\cdot,0.5)$, $Re = 5,000$, (DC0), (DC1), (C0) and (C1) (top to bottom).

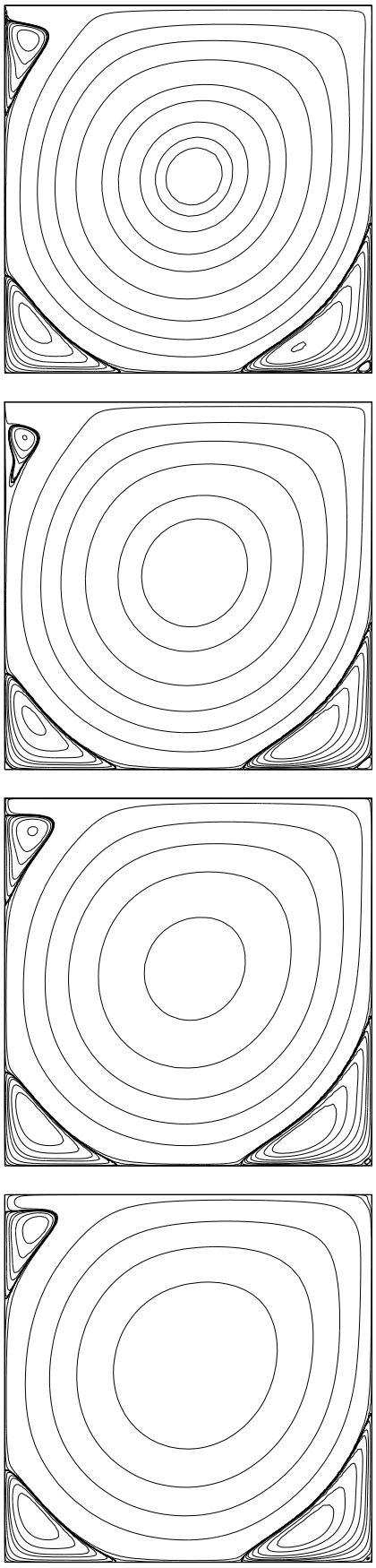

Figure 9: Streamlines, $Re = 5,000$, (DC0), (DC1), (C0) and (C1) (top to bottom).

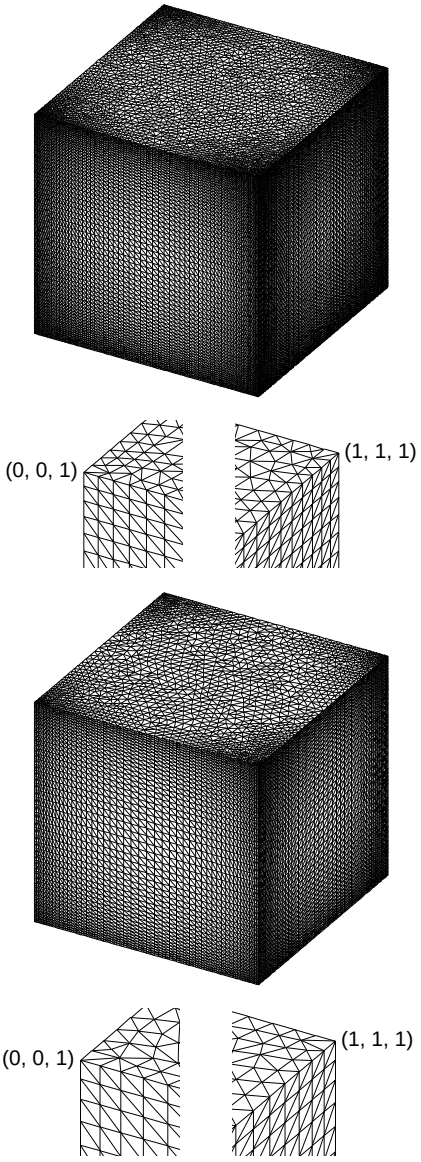

Figure 10: Meshes used for Problem 2, Fine mesh ($N_\Omega = 64$), the mesh magnified around the points $(x_1, x_2, x_3) = (0,0,1)$ and $(1,1,1)$, Coarse mesh ($N_\Omega = 48$) and the mesh magnified around the points (top to bottom).

Table 4: Discretization parameters for meshes in Fig 10.

Mesh	♯ of nodes	♯ of elements	$h_{\min}$
Fine	172,965	972,288	5.16×10^{-3}
Coarse	74,627	410,688	7.09×10^{-3}

Table 5: Convergence times.

		$t\ (\in \mathbb{N})$	
	Re	Fine mesh	Coarse mesh
(C0-3D):	100	12	12
	400	32	32
	1,000	58	58
(C1-3D):	100	11	11
	400	33	33
	1,000	53	53

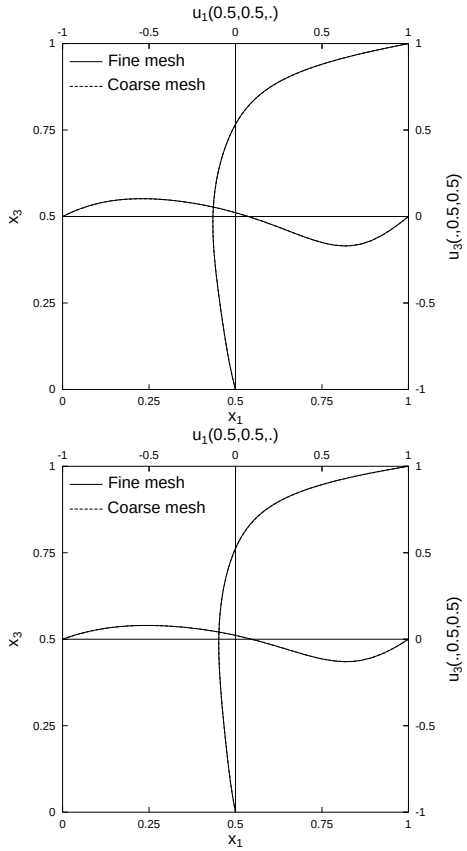

Figure 11: Graphs of $u_{h1}(0.5, 0.5, \cdot)$ and $u_{h3}(\cdot, 0.5, 0.5)$, $Re = 100$, (C0-3D) (top) and (C1-3D) (bottom).

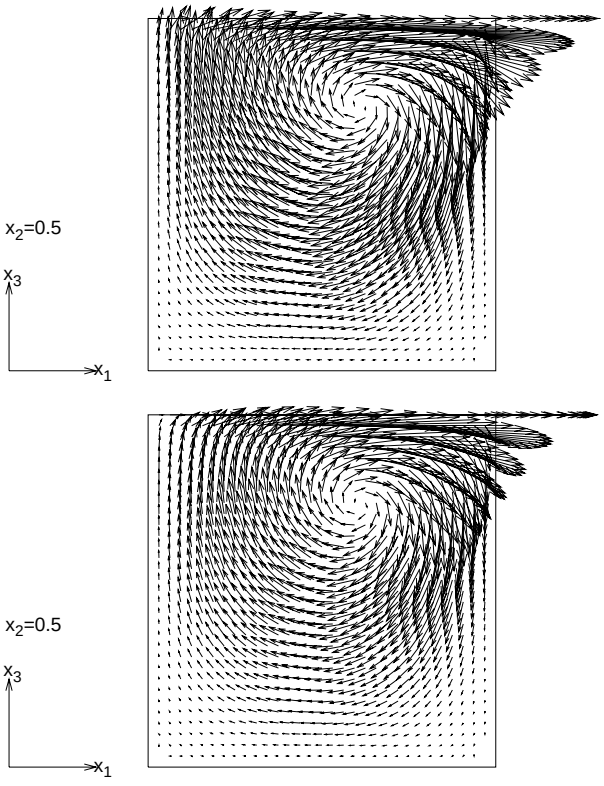

Figure 12: Projections of velocity vectors on the plane $x_2 = 0.5$, $Re = 100$, (C0-3D) (top) and (C1-3D) (bottom).

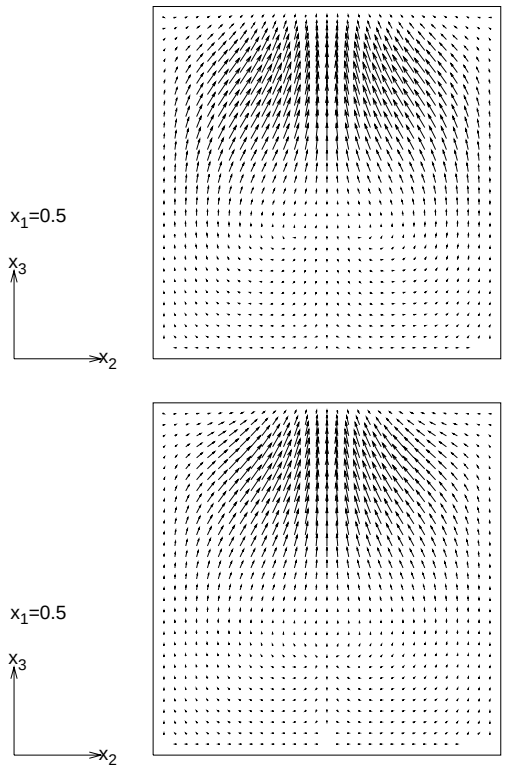

Figure 13: Projections of velocity vectors on the plane $x_1 = 0.5$, $Re = 100$, (C0-3D) (top) and (C1-3D) (bottom).

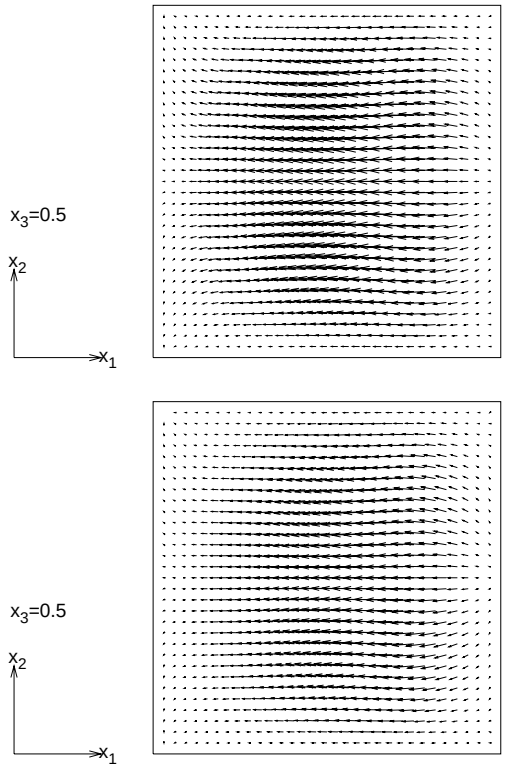

Figure 14: Projections of velocity vectors on the plane $x_3 = 0.5$, $Re = 100$, (C0-3D) (top) and (C1-3D) (bottom).

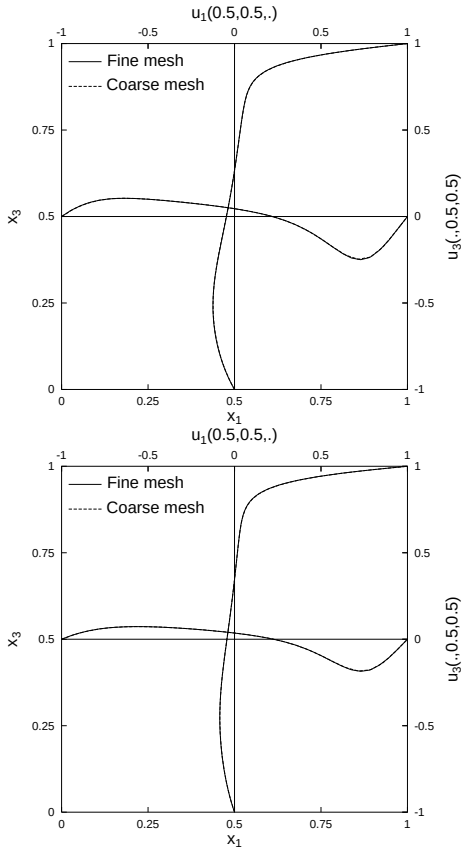

Figure 15: Graphs of $u_{h1}(0.5, 0.5, \cdot)$ and $u_{h3}(\cdot, 0.5, 0.5)$, $Re = 400$, (C0-3D) (top) and (C1-3D) (bottom).

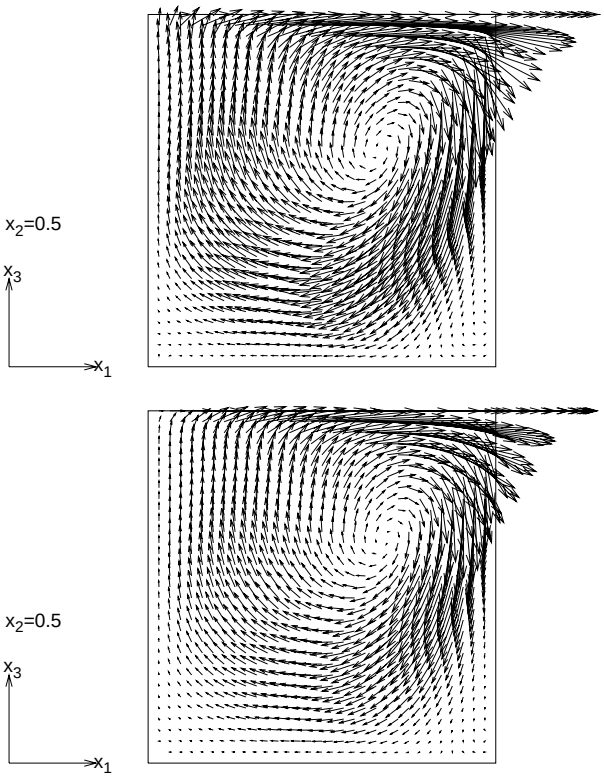

Figure 16: Projections of velocity vectors on the plane $x_2 = 0.5$, $Re = 400$, (C0-3D) (top) and (C1-3D) (bottom).

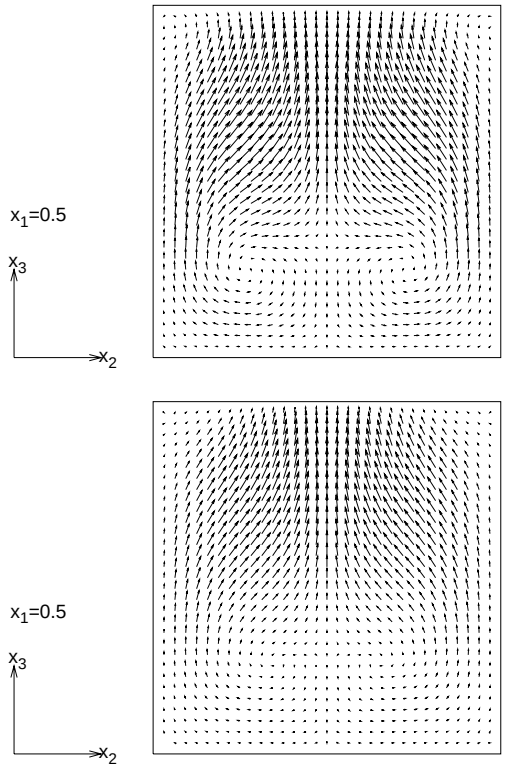

Figure 17: Projections of velocity vectors on the plane $x_1 = 0.5$, $Re = 400$, (C0-3D) (top) and (C1-3D) (bottom).

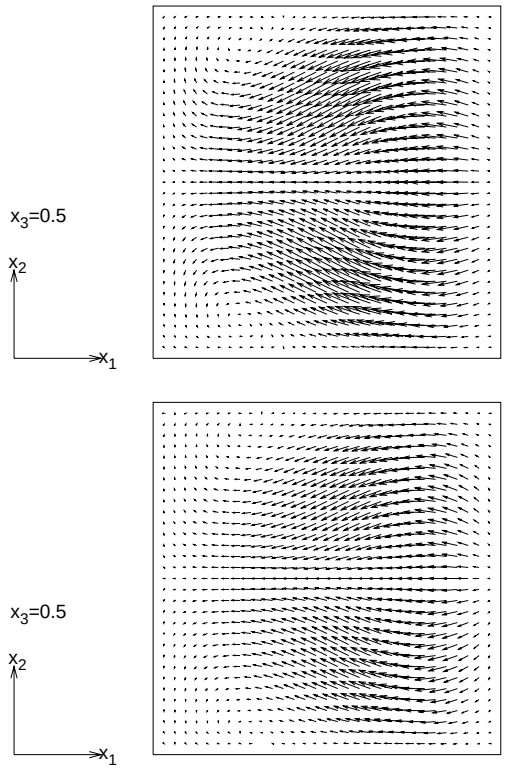

Figure 18: Projections of velocity vectors on the plane $x_3 = 0.5$, $Re = 400$, (C0-3D) (top) and (C1-3D) (bottom).

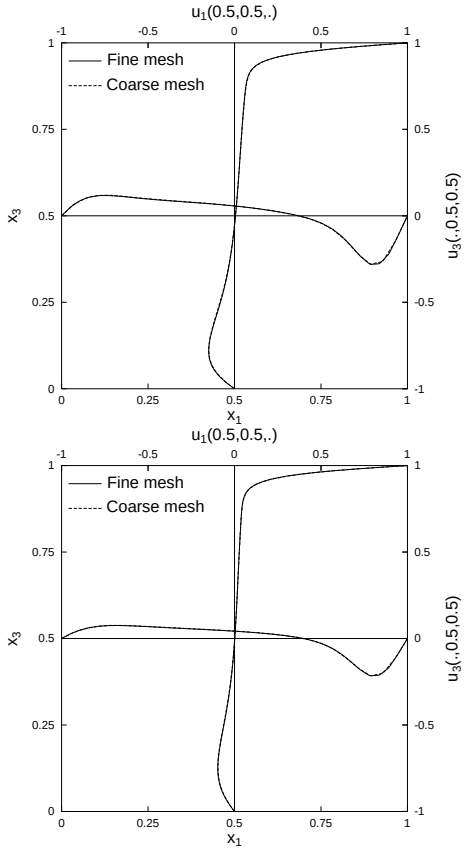

Figure 19: Graphs of $u_{h1}(0.5, 0.5, \cdot)$ and $u_{h3}(\cdot, 0.5, 0.5)$, $Re = 1,000$, (C0-3D) (top) and (C1-3D) (bottom).

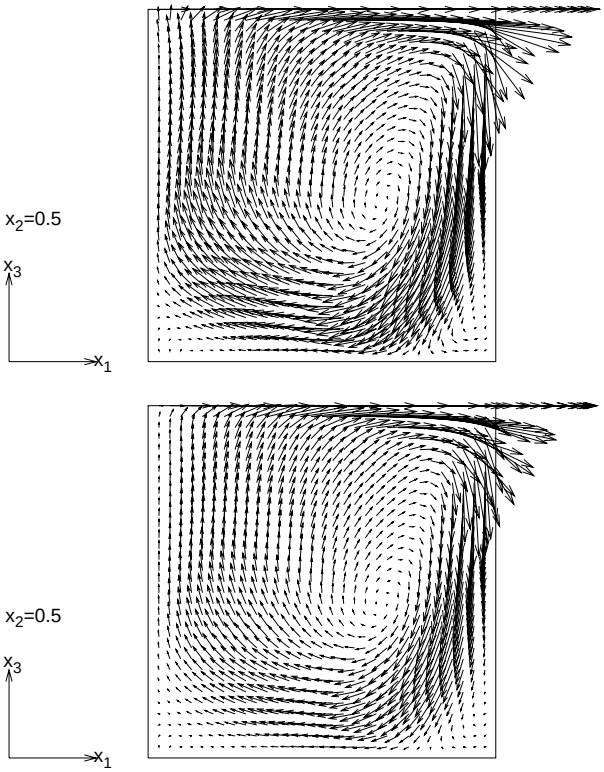

Figure 20: Projections of velocity vectors on the plane $x_2 = 0.5$, $Re = 1,000$, (C0-3D) (top) and (C1-3D) (bottom).

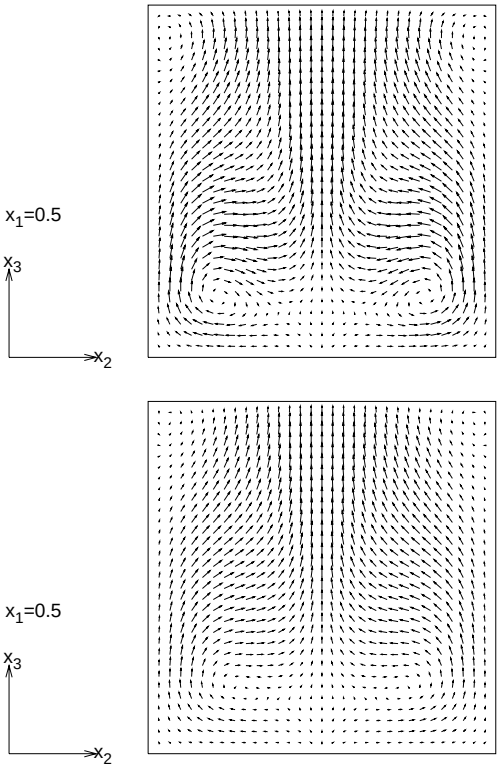

Figure 21: Projections of velocity vectors on the plane $x_1 = 0.5$, $Re = 1,000$, (C0-3D) (top) and (C1-3D) (bottom).

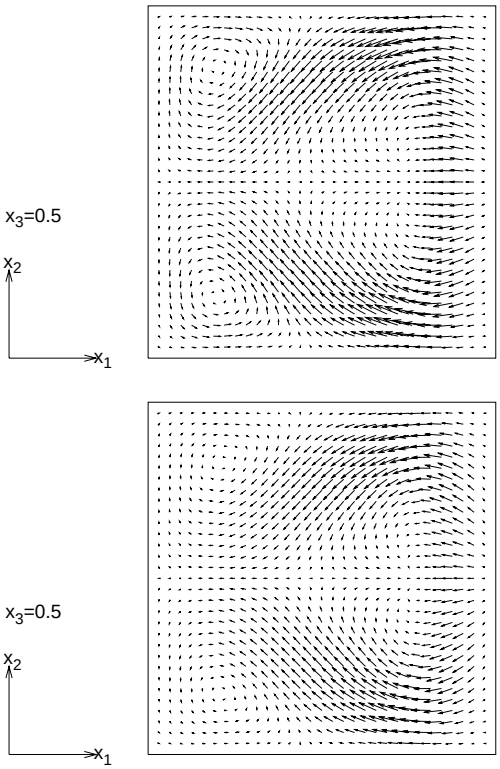

Figure 22: Projections of velocity vectors on the plane $x_3 = 0.5$, $Re = 1,000$, (C0-3D) (top) and (C1-3D) (bottom).

5 Conclusions

We have applied a newly developed characteristic-curve finite element scheme to cavity flow problems. The scheme uses a cheap element P1/P1 with pressure stabilization method, and the matrix of resulting linear system is symmetric and identical. Therefore, the scheme leads to symmetric linear solvers and easy large scale computations. We have solved two- and three-dimensional cavity flow problems with the Reynolds numbers up to 5,000 (2D) and 1,000 (3D). In the two-dimensional case, we have observed the difference of solutions by the three types of the Dirichlet boundary condition, discontinuous, C^0 and C^1 continuous ones. From the difference of the solutions of the problems with boundary conditions (DC0) and (DC1), we have seen the influence of the discontinuity of g_1. For problems with continuous boundary conditions in 2D and 3D, the streamlines and velocity vectors obtained have shown the flow patterns well. These results imply that the scheme can be applied for the practical problem.

The computations in this paper were carried out on IBM eServer p5 595 (power 5, 1.9GHz) with IBM XL C/C++ Enterprise Edition V7.0 at Research Institute for Information Technology of Kyushu University.

Acknowledgements. The author wishes to express his sincere thanks to Professor M. Tabata, Kyushu University for his continuous encouragement and stimulating discussions. This work was supported by the Japan Society for the Promotion of Science under Grant-in-Aid for Scientific Research (S), No. 16104001.

References

[1] Barrett, R., Berry, M., Chan, T. F., Demmel, J., Donato, J., Dongarra, J., Eijkhout, V., Pozo, R., Romine, C. and van der Vorst, H., *Templates for the Solution of Linear Systems: Building Blocks for Iterative Methods*, SIAM, Philadelphia, 1994.

[2] Boukir, K., Maday, Y., Métivet, B. and Razafindrakoto, E., A high-order characteristics/finite element method for the incompressible Navier-Stokes equations, *International Journal for Numerical Methods in Fluids*, **25**, 1997, pp. 1421–1454.

[3] Brezzi, F. and Douglas Jr., J., Stabilized mixed methods for the Stokes problem, *Numerische Mathematik*, **53**, 1988, pp. 225–235.

[4] Brezzi, F. and Fortin, M., *Mixed and Hybrid Finite Element Methods*, Springer, New York, 1991.

[5] Cruchaga, M. A. and Oñate, E., A finite element formulation for incompressible flow problems using a generalized streamline operator, *Computer Methods in Applied Mechanics and Engineering*, **143**, 1997, pp. 49–67.

[6] FreeFem++, http://www.freefem.org/.

[7] Fujima, S., Tabata, M. and Fukasawa, Y., Extension to three-dimensional problems of the upwind finite element scheme based on the choice of up- and downwind points, *Computer Methods in Applied Mechanics and Engineering*, **112**, 1994, pp. 109–131.

[8] Ghia, U., Ghia, K. N. and Shin, C. T., High-Re solutions for incompressible flow using the Navier-Stokes equations and a multigrid method, *Journal of Computational Physics*, **48**, 1982, pp. 387–411.

[9] Girault, V. and Raviart, P.-A., *Finite Element Methods for Navier-Stokes Equations, Theory and Algorithms*, Springer, Berlin, 1986.

[10] Iwatsu, R., Hyun, J. M. and Kuwahara, K., Analyses of three-dimensional flow calculations in a driven cavity, *Fluid Dynamics Research*, **6**, 1990, pp. 91–102.

[11] Jiang, B., Lin, T. L. and Povinelli, L. A., Large-scale computation of incompressible viscous flow by least-squares finite element method, *Computer Methods in Applied Mechanics and Engineering*, **114**, 1994, pp. 213–231.

[12] Kondo, N., Tosaka, N. and Nishimura, T., Third-order upwind finite element formulations for incompressible viscous flow problems, *Computer Methods in Applied Mechanics and Engineering*, **93**, 1991, pp. 169–187.

[13] Ku, H. C., Hirsh, R. S. and Taylor, T. D., A pseudospectral method for solution of the three-dimensional incompressible Navier-Stokes equations, *Journal of Computational Physics*, **70**, 1987, pp. 439–462.

[14] Mori, M., Sugihara, M. and Murota, K., *Matrix Computations*, Iwanami, Tokyo, 1994 (in Japanese).

[15] Nallasamy, M. and Prasad, K. K., On cavity flow at high Reynolds numbers, *Journal of Fluid Mechanics*, **79**, 1977, pp. 391–414.

[16] Notsu, H. and Tabata, M., A single-step characteristic-curve finite element scheme of second order in time for the incompressible Navier-Stokes equations, *Journal of Scientific Computing*, DOI 10.1007/s10915-008-9217-5.

[17] Notsu, H. and Tabata, M., A combined finite element scheme with a pressure stabilization and a characteristic-curve method for the Navier-Stokes equations, *Transactions of the Japan Society for Industrial and Applied Mathematics*, **18**, No. 3, 2008, pp. 427–445 (in Japanese).

[18] Pironneau, O., On the transport-diffusion algorithm and its applications to the Navier-Stokes equations. *Numerische Mathematik*, **38**, 1982, pp. 309–332.

[19] Pironneau, O., *Finite Element Methods for Fluids*, John Wiley & Sons, Chichester, 1989.

[20] Stroud, A. H., *Approximate calculation of multiple integrals*, Prentice-Hall, Englewood Cliffs, New Jersey, 1971.

[21] Süli, E., Convergence and nonlinear stability of the Lagrange-Galerkin method for the Navier-Stokes equations, *Numerische Mathematik*, **53**, 1988, pp. 459–483.

[22] Tabata, M., Discrepancy between theory and real computation on the stability of some finite element schemes, *Journal of Computational and Applied Mathematics*, **199**, 2007, pp. 424–431.

[23] Tabata, M. and Fujima, S., An upwind finite element scheme for high-Reynolds-number flows, *International Journal for Numerical Methods in Fluids*, **12**, 1991, pp. 305–322.

[24] Tabata, M. and Fujima, S., Robustness of a characteristic finite element scheme of second order in time increment, in *Computational Fluid Dynamics 2004*, editors Groth, C. and Zingg, D. W., Springer, Berlin, 2006, pp. 177–182.

List of MI Preprint Series, Kyushu University

The Grobal COE Program
Math-for-Industry Education & Research Hub

MI

2008-1 Takahiro Ito, Shuichi Inokuchi & Yoshihiro Mizoguchi
Abstract collision systems simulated by cellular automata

2008-2 Eiji Onodera
The intial value problem for a third-order dispersive flow into compact almost Hermitian manifolds

2008-3 Hiroaki Kido
On isosceles sets in the 4-dimensional Euclidean space

2008-4 Hirofumi NOTSU
Numerical computations of cavity flow problems by a pressure stabilized characteristic-curve finite element scheme